J Mol Model (2014) 20:2526
DOI 10.1007/s00894-014-2526-8

ORIGINAL PAPER

Synthesis, characterization, and computational study of a new dimethoxy-chalcone

Ricardo R. Ternavisk · Ademir J. Camargo · Francisco B. C. Machado · José A. F. F. Rocco · Gilberto L. B. Aquino · Valter H. C. Silva · Hamilton B. Napolitano

Received: 30 April 2014 / Accepted: 10 November 2014 / Published online: 25 November 2014

Abstract Chalcones are an important class of medicinal compounds and are known for taking part in various biological activities as in anti-inflammatory, anti-leishmania, antimitotic, and antiviral. Chemically, chalcones consist of open-chain flavonoids in which the two aromatic rings are joined by a three-carbon α,β-unsaturated carbonyl system. The wide action spectrum has attracted our attention to synthesize, crystallize, and characterize the dimethoxy-chalcone $C_{18}H_{18}O_3$. Aiming to understand the process of crystal lattice stabilization, a combination of technique has been used including X-ray diffraction, infrared spectroscopy and computational molecular modeling. The theoretical calculations were carried out by the density functional method (DFT) with the M06-2X functional, with the 6-311+G(d,p) basis set. The vibrational wavenumbers were calculated and the scaled values were compared with experimental FT-IR spectrum. The intermolecular interactions were quantified and intercontacts in the crystal structure were analyzed using Hirshfeld surfaces. Bond distances and angles described by the X-ray diffraction and theoretical calculation are very similar. The C-H….O contacts contributing to assemble the supramolecular architecture are also responsible for the molecular structure assembly.

This paper belongs to Topical Collection Brazilian Symposium of Theoretical Chemistry (SBQT2013)

R. R. Ternavisk · A. J. Camargo · G. L. B. Aquino · V. H. C. Silva · H. B. Napolitano (✉)
Ciências Exatas e Tecnológicas, Universidade Estadual de Goiás, CP459, 75001-970 Anápolis, GO, Brazil
e-mail: hbnapolitano@gmail.com

F. B. C. Machado · J. A. F. F. Rocco
Departamento de Química, Instituto Tecnológico de Aeronáutica, 12228-900 São José dos Campos, SP, Brazil

V. H. C. Silva
Faculdade de Tecnologia SENAI Roberto Mange, 75113-630 Anápolis, GO, Brazil

Keywords DFT · Dimethoxy-chalcone · Infrared spectroscopy · X-ray diffraction

Introduction

Chalcones are considered key precursors for flavonoid and isoflavonoid syntheses. It can be obtained from natural sources or synthetic route. The basic structure of chalcones consists of the two aromatic rings joined by a three-carbon α,β-unsaturated carbonyl system [1, 2]. Chalcones have received great attention due to their relatively simple synthesis process, simple structure, and a range of pharmacological activities have been reported such as: anticancer [3], anti-leishmanial and antimalarial [4], antiviral [5], and other bioactivities etc. [1]. Dimethoxy and trimethoxy chalcone derivatives have been reported in the literature as effective anti-inflammatory agents [6]. The chalcones versatility are attributed to the α,β unsaturated ketone moiety, the conjugated double bonds and the completely delocalized pi electron system on both aromatic rings. The large range of pharmacological properties of chalcones is intrinsically linked to the substitution pattern of the two aromatic rings [7]. Fundamental properties of the material such as stability, solubility, color, strength and furthermore, pharmacological/technological application are related with the molecular arrangement in the crystal lattice [8, 9].

In view of the numerous important biological activities of chalcones, as described before, there is considerable interest in the scientific community in synthesizing new chalcone derivatives suitable for biological applications. Bearing this in mind, this paper presents the results of the synthesis, structural characterization, and M06-2X/6-311+G(d,p) calculations of (E)-3-(3,5-dimethoxyphenyl)-1-(4-methylphenyl)prop-2-en-1-one ($C_{18}H_{18}O_3$). In order to understand the nature of crystal packing and to describe the molecular sites where

electrophilic and nucleophilic reactions can take place and the hydrogen-bonding interactions, the molecular electrostatic potential mapping was performed on title compound at the same level of theory. The M06-2X/6-311+G(d,p) calculations of the vibrational modes were carried out in order to support the spectrum assignment of the (E)-3-(3,5-dimethoxyphenyl)-1-(4-methylphenyl)prop-2-en-1-one. Finally, the computations of the geometric and electronic properties presented here are very important to shed light on the understanding of the structure-activity relationship [10] for this new compound.

Experimental and computational procedures

Synthesis and crystallization

In a 25 mL flask were added 0.3003 g (2.24 mmol) of 4-methylacetophenone **2** and cooled in an ice bath. Then, 9 ml of a solution of NaOH (50 %*w/v*) was added, and then 0.41 g (2.24 mmol) of 3,5-dimethoxybenzaldehyde **3** was added (Scheme 1). The resulting solution was stirred at room temperature for 24 h, after this time the medium reaction was poured into ice water and neutralized with 50 % HCl solution. The resulting precipitate was filtered, washed with water and purified by recrystallization from methanol. The solid obtained showed yellow coloration: *mp*.: 85.2–87.6 ° C. **^{1}H-NMR (500 MHz) ($CDCl_3$):**δ (*ppm*) 2,46 (s, 3 H, C*H*$_3$Ph) 3,86 (s, 6 H, OC*H*$_3$Ph) 6,55 (t, 1H, *Ph*CH, *J*=2,4 Hz) 6,80 (d, 2H, *Ph*CH, *J*= 2,4 Hz) 7.33 (d, 2 H, *Ph*OCH$_3$,*J*=8.4 Hz) 7.50 (d, 1H, C*H*CO, *J*=15.6 Hz) 7.73 (d, 1H, C*H*Ph, *J*=15.6 Hz) 7.95 (d, 2H, *Ph*OCH$_3$, *J*=8.4 Hz). **^{13}C-NMR (125 MHz) ($CDCl_3$):**δ 21,53 ***C***H$_3$Ph 55,66 (O***C***H$_3$Ph) Anel ***Ph***. (102,85; 106,52; 128,85; 129,50; 135,78; 137,11; 161,26) **olefin**. (122,88; 144,48) 190,28 (***C***=O). **IR (KBr) cm^{-1}**: 2940; 1657 (C=O); 1593; 1426. The compound $C_{18}H_8O_3$(**1**) was crystallized from methanol in 5 days by the slow evaporation technique.

Crystallographic and infrared spectroscopy characterization

The X-ray diffraction data for the title compound were collected at room temperature using a KAPPA-CCD diffratometer [11] with graphite-monochromated MoKα radiation (λ=0.71073 Å). The structure (Fig. 1) was solved by direct methods and anisotropically refined with full-matrix least-squares on F^2 using SHELXL97 [12]. The hydrogen atoms on the carbon atoms were positioned geometrically and refined applying the riding model [C-H 0.93 Å for C sp^2 and C-H 0.96 Å for C sp^3] with *U*iso(H)=1.2*U*eq(C) for C sp^2 and *U*iso(H)=1.5*U*eq(C) for C sp^3. The crystallographic data of $C_{18}H_{18}O_3$ are *a*=16.848(2) Å, *b*=11.539(2) Å, *c*=8.089(2) Å, β =103.507(5)°, cell volume V=1529.18(6) Å^3, monoclinic space group P2$_1$/c, goodness of fit 1.020, and *R*=0.048 (Table 1). The cell refinements were carried out using the software Collect [13] and Scalepack software [14]. Data reduction was carried out using the software Denzo-SMN and Scalepack software [14]. Molecular representation, tables and pictures were generated by WinGX [15], ORTEP-3 [16], and MERCURY 2.2 [17] programs. The intermolecular interactions of the title compound are quantified using PARST of WingX packing and intercontacts in the crystal structure are analyzed using Hirshfeld surfaces. The Hirshfeld surfaces [18, 19] and the associated 2D fingerprint plots were calculated using Crystal Explorer [20]. This approach is a graphical tool for visualization and understanding of intermolecular interactions [20].

The experimental absorption spectrum in the solid state was observed in the region (4000–400 cm^{-1}) obtained in a spectrophotometer FT-NIR/MIR PerkinElmer Frontier, the sample was screened in potassium bromide (KBr) and the main absorbent groups were characterized. The experimental infrared spectrum of $C_{18}H_{18}O_3$ is presented in Fig. 4(a).

Computational procedures

The start geometry used in the calculations was taken directly from the x-ray data and it was fully optimized without constraint using the density functional theory (DFT) as implemented in the Gaussian 09 package of programs [21, 22]. The hybrid meta-GGA exchange correlation functional M06-2X [23] was employed throughout the calculations. This functional is parameterized for nonmetals and it is recommended for applications involving main group thermochemistry, kinetics, non covalent interactions, and electronic excitation energies [23, 24]. The extended Gaussian basis set 6-311+G(d,p) of Pople and coworkers [25, 26] was used for all the computations. To confirm if the fully optimized geometry found in a local minimum, analytic harmonic frequency calculations were carried out at the same level of theory. The absence of imaginary frequencies shows that the optimized structure is really in a local minimum. The assignments of the vibrational modes were supported by the

Scheme 1 Synthesis of dimethoxy-chalcone C18H18O3

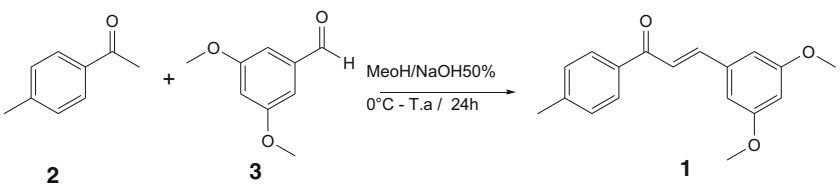

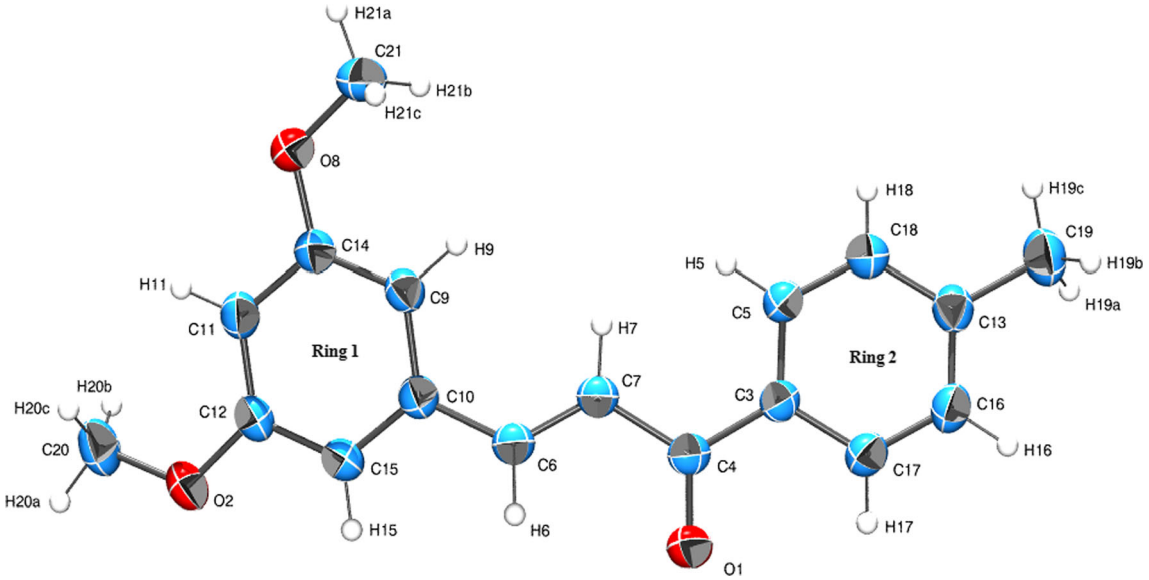

Fig. 1 The ORTEP diagram of ellipsoids at 30 % probability level with the atomic numbering scheme for $C_{18}H_{18}O_3$. All bonds are in the normal range and hydrogen atoms are shown as spheres of arbitrary radii

animation option of Gassview [24], which is a graphical interface for Gaussian program that can provide us with a visual representation of the shape of the vibrational modes.

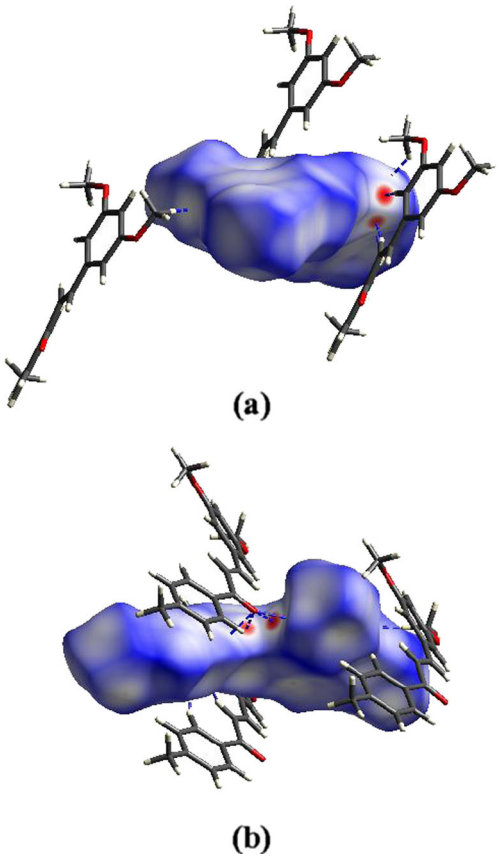

Fig. 2 Hirshfeld surfaces indicating intermolecular contacts for $C_{18}H_{18}O_3$. Dotted lines represent hydrogen bonds

In order to investigate the reactive site of the (E)-3-(3,5-dimethoxyphenyl)-1-(4-methylphenyl)prop-2-en-1-one compound the molecular electrostatic potential (MEP) was evaluated at the M06-2X/6-311+G(d,p) level of theory. The mapping of the molecular electrostatic potential around a molecule was obtained using the equation [27]:

$$V(\boldsymbol{r}) = \sum \frac{Z_A}{|\boldsymbol{R}_A - \boldsymbol{r}|} - \int \frac{\rho(\boldsymbol{r}')}{|\boldsymbol{r}' - \boldsymbol{r}|} d\boldsymbol{r}',$$

Table 1 Crystal data and structure refinement for $C_{18}H_{18}O_3$

Formula weight	282.32 u.a.
Temperature	293 K
Wavelength	0.71073 Å
Crystal system	Monoclinic
Space group	$P2_1/c$
Unit cell dimensions	a =16.8489(4) Å
	b =11.5390(3) Å
	c =8.0891(2) Å
	β=103.506(2)^0
Volume	1529.18 Å^3
Z, calculated density	4, 1.29 mg/m^3
Absorption coefficient	0.083 mm^{-1}
F(000)	600.0
Reflections collected/unique	30,952/3127
Refinement method	Direct methods
Goodness-of-fit on F^2	1.020
Final R indices [I >2σ(I)]	0.048
R indices (all data)	0.0744

where $V(\boldsymbol{r})$ stands for the electrostatic potential at point $\boldsymbol{r}$ created by nuclei and electrons of the molecular system, Z_A is the charge of nucleus A located at $\boldsymbol{R}_A$, $\rho(\boldsymbol{r}')$ is the electronic density, and $\boldsymbol{r}'$ is the integration variable. The MEP mapping is a very powerful tool to describe molecular sites of electrophilic attack, nucleophilic reactions, and hydrogen bonding interaction. In addition, the molecular electrostatic potential map is commonly used to describe drug-receptor and enzyme-substrate interactions, because it is the driving force that acts on long distance.

Results and discussion

Crystallographic structure

The dimethoxy-chalcone $C_{18}H_{18}O_3$ crystallizes in the centrosymmetric space group $P2_1/c$. The molecule is a chalcone with 3,5-dimethoxyphenyl and 4-methylphenyl rings bonded at the opposite ends of a –CO–CH=CH– group. The ellipsoid displacement plot with the numbering scheme is presented in Fig. 1. X-ray geometry parameters (bond lengths, bond angles, and torsion angles) were compared with fully optimized geometric parameters, and the results are very similar. The most notable discrepancies are observed for C4-O1 and C5-C18 bonds [1.228(2) Å and 1.214 Å / 1.377(2) Å and 1.391 Å, respectively] and C4-C7-C6 angle [121.5(1)° and 120.04°, respectively]. The differences occur because the X-ray results belong to the solid phase while optimized geometry was carried out at free molecule in vacuum. The benzene rings 1 and 2 are planar with a mean deviation of 0.0095 Å and 0.0054 Å respectively. The planes between the two benzene rings form a dihedral angle of 28.45(4)° for packing and 12.86° for the M06-2X/6-311+G (p,d) optimized structure. The torsion angles for –C6=C7–C4–C3 are −175.33°, −179.22° and 167.58°, 177.09° for –C10–C6=C7–C4, respectively. The optimized and experimental geometry are presented in Table 2.

The potential intermolecular interactions of the title compound are visualized using Hirshfeld surface analysis. This

Table 2 The calculated and experimental geometric parameters for $C_{18}H_{18}O_3$

Bond distances (°Å)	X-ray	DFT	Bond angles (°)	X-ray	DFT
C3-C5	1.387(2)	1.394	C12-O2-C20	117.8(1)	117.7
C3-C17	1.397(2)	1.398	C4-C3-C5	123.4(1)	122.8
C3-C4	1.486(2)	1.498	C4-C3-C17	118.9(1)	118.2
C4-O1	1.228(2)	1.214	C5-C3-C17	117.6(1)	118.9
C4-C7	1.477(3)	1.488	O1-C4-C3	120.1(1)	120.3
C5-C18	1.377(2)	1.391	O1-C4-C7	120.4(1)	121.5
C6-C7	1.327(3)	1.338	C3-C4-C7	119.4(1)	118.1
C6-C10	1.465(2)	1.468	C3-C5-C18	121.2(1)	120.4
C9-C14	1.377(2)	1.384	C7-C6-C10	127.2(1)	126.8
C9-C10	1.406(2)	1.408	C4-C7-C6	121.5(1)	120.1
C10-C15	1.393(2)	1.386	C14-O8-C21	117.9(1)	117.8
C11-C12	1.377(3)	1.384	C10-C9-C14	118.7(1)	119.1
C11-C14	1.394(2)	1.403	C6-C10-C15	118.1(1)	118.1
C12-O2	1.365(2)	1.355	C9-C10-C15	120.1(1)	120.1
C12-C15	1.393(2)	1.401	C12-C11-C14	119.5(1)	119.2
C13-C18	1.387(3)	1.393	O2-C12-C11	124.5(1)	124.1
C13-C16	1.387(2)	1.399	O2-C12-C15	115.3(1)	115.6
C13-C19	1.505(2)	1.506	C11-C12-C15	120.2(1)	120.2
C14-O8	1.366(2)	1.357	C16-C13-C18	117.5(1)	118.4
C16-C17	1.372(2)	1.384	C16-C13-C19	121.6(2)	120.3
C20-O2	1.425(3)	1.413	C18-C13-C19	120.9(2)	121.3
C21-O8	1.425(2)	1.412	O8-C14-C9	124.3(1)	124.3
			O8-C14-C11	114.4(1)	114.5
			C9-C14-C11	121.3(1)	121.1
			C10-C15-C12	120.1(1)	120.1
			C13-C16-C17	121.8(1)	120.9
			C3-C17-C16	120.7(2)	120.4
			C5-C18-C13	121.2(1)	120.9

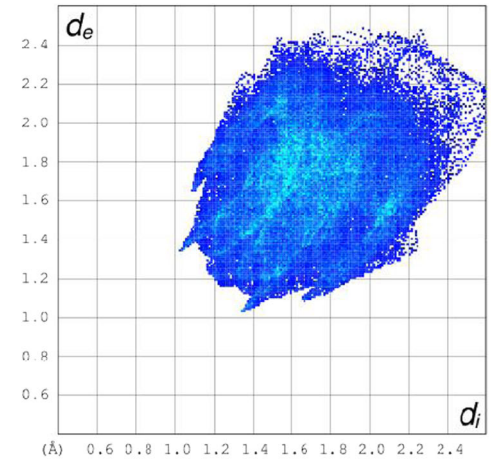

(a)

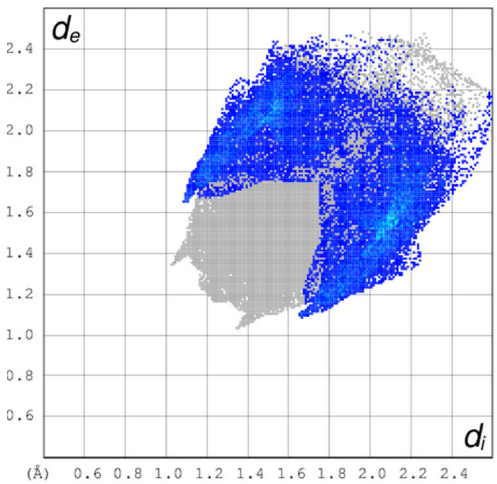

(b) C….H

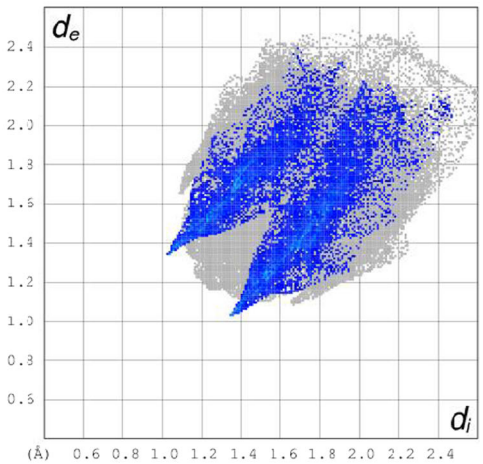

(c) O….H

Fig. 3 **a** Fingerprint of the $C_{18}H_{18}O_3$. **b** C…H, **c** O…H. The outline of the full fingerprint is shown in gray. d_i the closest internal distance from a given point on the Hirshfeld surface and d_e is the closest external contacts

approach is a graphical tool for visualization and understanding of intermolecular interactions. The intermolecular contacts are estimated using WingX. The chart indicates the contribution of intercontacts to the Hirshfeld surfaces. The Hirshfeld surface is a measurement of the space occupied by a given molecule in the crystal and summarizes information from all interactions and molecular contacts simultaneously [19]. The two-dimensional fingerprint plots are derived from the Hirshfeld surface, which provide a summary of the frequency of each combination of d_e (*i.e.*, the distance from the surface to the nearest atom in the molecule itself) and d_i (*i.e.*, distance from the surface to the nearest atom in another molecule) across the surface of a molecule. Two-dimensional fingerprint plots were generated by using the d_i and d_e pairs measured on each individual spot of the calculated Hirshfeld surface. This information shows not only the set of present interactions, but also the relative area of the surface corresponding to each interaction. Blue color corresponds to the low frequency of occurrence of (d_e, d_i) pair, while red points indicate the high frequency of the surface points with that (d_e, d_i) combination.

These intercontacts are highlighted by conventional mapping of d_{norm} (*i.e.*, the normalized contact distance) on molecular Hirshfeld surfaces are shown in Fig. 2. The red spots over the surface indicate the intercontacts involved in the hydrogen bonds. Furthermore, intercontacts were plotted with fingerprint plots in Fig. 3. The intercontacts C…H (Fig. 3(b)) showing presence of O…H contact with the two characteristic wings, intercontacts O…H (Fig. 3(c)) showing two narrow pointed wings provide evidence for C-H…O non-classical hydrogen [17]. The non-classical hydrogen bonds are presented in Table 3.

The electrostatic potential surface shows that the regions close to the oxygen atoms have negative charge density. However, the region close to the hydrogen H9, H7, and H5 atoms present high concentration of positive charges. This region is the most provable place to occur interactions like the ones involved in packing. The Hirshfeld surface analysis, with finger plots and electrostatic potential map, reveals the intermolecular contacts and distribution of electrostatic potential of the title compound. It helps to understand the molecules packing and the crystal stabilization.

Infrared spectrum

The vibrational frequencies (theoretical and experimental) in the infrared range, are in good agreement, from which it was possible to characterize the main absorbent groups. The observed discrepancies are due to the fact that calculations were made for a free molecule in a vacuum, while experiments were carried out in a solid sample. The calculated vibrational frequencies for the optimized geometries and the proposed vibrational assignments as well as IR intensities are given in Table 4. The spectrum is presented in Fig. 4. It is well known

Table 3 Non-classical hydrogen bond for $C_{18}H_{18}O_3$

D-H … A (Å)	D-H (Å)	H-A (Å)	D-A (Å)	D-H …A (°)	Symmetry codes
C9-H9 …O1	0.930(1)	2.528(1)	3.456(2)	175.82(1)	x,-y+1/2+1,+z-1/2
C7-H7 …O1	0.930(1)	2.571(1)	3.472(2)	163.26(1)	x,-y+1/2+1,+z-1/2
C5-H5 …O1	0.930(2)	2.800(1)	3.588(2)	143.14(1)	x,-y+1/2+1,+z-1/2
C21-H21 …O1	0.960(2)	2.7321)	3.388(2)	126.17(2)	x,-y+1/2+1,+z-1/2
C20-H20 …O2	0.960(2)	2.701(1)	3.658(2)	173.23(2)	x-1/2,-y+1/2,z

that the DFT calculations overestimate the vibrational frequencies systematically [28], and the use of a proper scaling factor for M06-2X, equal to 0.947 [29] provides more reliable values to compare to the experimental data.

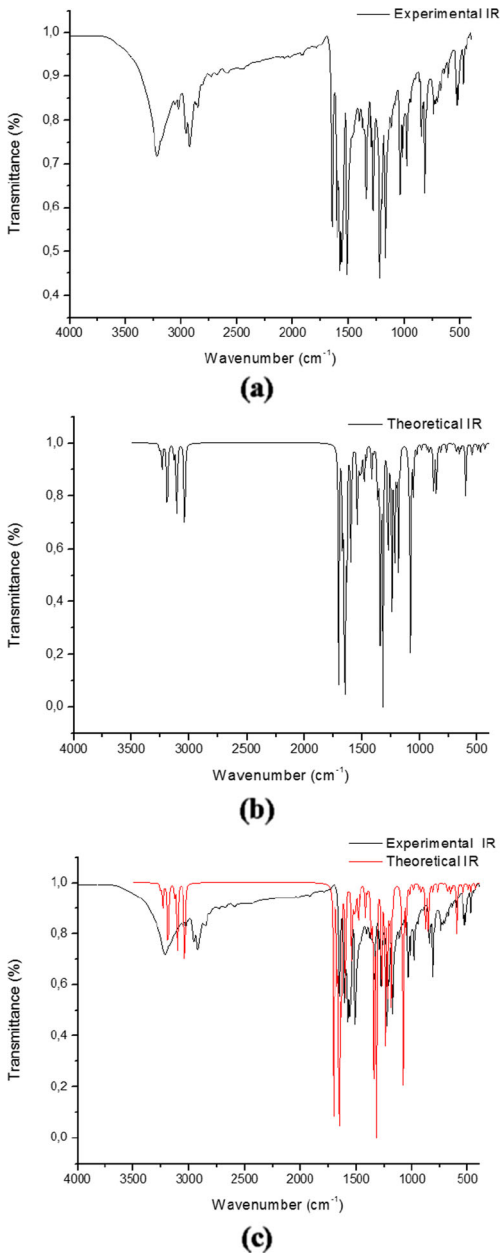

Fig. 4 The experimental (**a**), theoretical (**b**), and overlap (**c**) of infrared spectrum of $C_{18}H_{18}O_3$

The heteroaromatic structure shows the presence of CH stretching vibrations in the 3000–3175 cm^{-1} range, which is the characteristic region for the identification of CH stretching vibrations [30]. In this region, the bands are not affected appreciably by the nature of the substituents. The ring CC stretching vibrations occur in the region 1321–1686 cm^{-1} [30, 31]. The CC stretching modes for the R1 and R2 rings are observed at 1527 and 1686 cm^{-1}. The ring stretching vibrations, which are highly characteristic of the aromatic ring itself, are very important in the spectrum of benzene and its derivatives. The prominent band between 1625 and 1650 cm^{-1} is characteristic of the α, β-unsaturated carbonyl group of a chalcone. In the present work, the calculated values are 1701 cm^{-1} for unscaled and 1611 cm^{-1} for scaled frequency. The band in 1792 cm^{-1} is characteristic of the C=O stretching mode [30].

Frontier molecular orbitals

The highest occupied molecular orbital (HOMO) and the lowest unoccupied molecular orbital (LUMO) energies are directly related to the ability to donate and accept electrons. The LUMO energy is directly related with the molecular electron affinity and characterizes the susceptibility of the molecule toward an attack by a nucleophile. Both the HOMO and the LUMO energies are important in radical reactions [32]. The energy difference between HOMO and LUMO is an important chemical stability index [33]. A large HOMO-LUMO gap implies high stability with respect to chemical reaction [34]. They are also used to describe chemical softness and hardness.

Figure 5 shows a graphical representation of the distribution and energy levels for HOMO and LUMO orbitals computed at the M06-2X/6-311+G(d,p) level of theory for (E)-3-(3,5-dimethoxyphenyl)-1-(4-methylphenyl)prop-2-en-1-one compound. The plot of the frontier molecular orbital helps us to have a better understanding of the nature of the chemical bond scheme [35]. As can be seen in Fig. 5, the HOMO (−8.7828 eV) orbital is localized entirely on the R1 ring (dimethoxyphenyl group), while the LUMO (−6.4783 eV) orbital is spread out throughout the molecule, except for the

Table 4 Vibrational assignments, experimental and calculated wave numbers in cm^{-1} of $C_{18}H_{18}O_3$ at M062X/6-311+G(d,p)

Mode no.	Unscaled freq.	Scaled freq.[a]	$I^{Infrared}$	FT-IR[b]	IR assigments
1	10	9	0.82		Γ $CCCC_{R2}$+Γ$CCCC_{R1}$
2	32	30	0.2		Γ CC-CC_{R2}+Γ CC-CC_{R1}
3	40	38	0.2		Γ $CCCC_{R2}$
4	58	54	0.3		ΓCH_3-O+Γ$CCCC$
5	84	80	1.2		ΓCH_3-O+ C_6H_6+ C_7H_7
6	91	86	5.5		Γ CH_3-O_8
7	97	91	0.2		Γ CH_3-O+t CH_3-C
8	102	96	2.4		Γ CH_3-O_2+t CH_3-C
9	109	104	1.0		t CH_3-C
10	167	158	0.5		ΓCH_3-O_8+ C_6H_6+ C_7H_7
11	170	161	1.2		Γ CH_3-O
12	204	193	1.0		t CH_3-O_2
13	211	199	0.6		t CH_3-O_8+ΓCCC
14	215	204	1.6		Γ CH_3-O
15	244	231	6.1		Γ$CCCC$+Γ CH_3-O
16	273	259	1.7		tCH_3-O_2
17	282	267	1.5		tCH_3-O+Γ$CCCC$
18	290	275	0.7		Γ $CCCC_{R1}$+tCH_3-O_2+tCH_3-O_8
19	291	275	0.5		tCH_3-O_2+tCH_3-O_8
20	330	313	0.2		Γ COC+ΓCOC
21	359	340	4.2		r CH_3
22	382	362	0.1		Γ$CCCC$+ΓCOC
23	414	392	0.6		$CCCC_{R2}$
24	439	416	2.9		β CCC_{R2}+β COC_{R1}
25	463	438	11.1		β CCC_{R1}+ CCC_{R2}
26	491	465	8.8	472(vw)	β CCC_{R1}+Γ$CCCC_{R2}$
27	532	504	2.8		Γ CCC_{R1}+β CCC_{R2}
28	550	521	9.1		R1 deformation
29	584	553	12.9		$C_{15}H_{15}$+ C_9H_9+Γ CC_{R1}
30	598	566	34.3	528(w)	β CCC_{R2}+r C=O
31	629	596	0.2		$C_{15}H_{15}$+ C_9H_9
32	640	606	0.5		Γ R1+R2 deformation
33	649	614	0.5	607(w)	R2 deformation
34	657	622	16.7		R2 and R1 deformation
35	682	646	20.9		CH_{R1}
36	708	670	3.0		R2 deformation
37	756	716	13.4		C_5H_5+ $C_{17}H_{17}$+ CC_{R2}
38	811	768	10.1	739(s)	R2 deformation+ν C_{13}-C_{19}
39	832	788	33.7		CH
40	845	800	26.9		CH_{R2}+ C_7H_7+ C_6H_6
41	855	809	37.3	814(m)	$C_{11}H_{11}$
42	871	825	6.2		CH_{R2}
43	876	829	8.0		$C_{15}H_{15}$+ $C_{16}H_{16}$+ $C_{17}H_{17}$
44	883	836	8.1	845(w)	νC4-C3 $C_{18}H_{18}$+ $C_{17}H_{17}$
45	913	865	2.7		$C_{15}H_{15}$+ $C_{16}H_{16}$+ C_7H_7
46	975	923	24.8		ν C-O-C
47	988	936	0.2		CH_{R1}
48	1008	955	7.9		ω CH_3–C+R1 deformation
49	1010	957	2.3		ω CH_3–C

Table 4 (continued)

Mode no.	Unscaled freq.	Scaled freq.[a]	$I^{Infrared}$	FT-IR[b]	IR assigments
50	1013	959	0.1		CH_{R2}
51	1018	964	5.4		$C_{16}H_{16}$+ $C_{17}H_{17}$
52	1027	973	31.6		C_6H_6+ C_7H_7
53	1038	983	32.1	979(m)	R2 deformation
54	1067	1010	19.8		ω CH_3 – C
55	1068	1012	87.1	1016(w)	ν C_7-C_4
56	1115	1056	36.9	1038(m)	ν C_{20}-O_2+β CH_{R1}
57	1123	1064	22.0		ν C_{21}-O_8+β CH_{R1}
58	1142	1082	4.7		β CH_{R2}
59	1180	1118	1.0		ω CH_3 – O_2
60	1187	1124	1.0		ω CH_3 – O_8
61	1188	1125	4.2		ν C-O+ν C_{10}-C_6
62	1206	1142	83.1		ν C-O+β C_9H_9+ β $C_{11}H_{11}$
63	1209	1145	49.0		β CH_{R1}
64	1222	1157	15.9		ω CH_3 – O_2+ω CH_3 – O_8
65	1245	1179	44.3	1171(s)	ν C_{13}-C_{19}+ β C_6H_6+β C_7H_7
66	1251	1185	181.1		β C_6H_6+ β C_7H_7+β C_9H_9+β CH_{R2}
67	1257	1190	147.7		ω CH_3–O_2+ω CH_3–O_8
68	1279	1211	8.8	1221(vs)	β CH_{R1}
69	1321	1251	519.0		β C_4-C_3+ β C_6H_6+β C_7H_7
70	1327	1257	6.9		ν CC_{R2}+β C_7H_7+β C_6H_6
71	1339	1268	4.5		ν CC_{R2}
72	1342	1271	2.7		ν CC_{R1}+ ν CC_{R2}
73	1360	1288	104.0	1280(vs)	β CH_{R2}+β C_6H_6+β C_7H_7
74	1419	1343	2.6		ω CH_3 – C
75	1421	1345	81.5		ν CC_{R1}+ν C_{10}- C_6+ω CH_3-O
76	1448	1371	13.0		ν CC_{R2}+β CH_{R2}
77	1474	1396	50.4		ω CH_3
78	1490	1411	11.0		ω CH_3
79	1493	1414	7.9		ν sym CH_3
80	1504	1424	14.6		ρ CH_3 – C
81	1504	1425	10.9		ρ CH_3 – O_2
82	1508	1428	41.5		ρ CH_3
83	1509	1429	45.9		ρ CH_3
84	1513	1433	15.0		ρ CH_3
85	1520	1439	39.0		ρ CH_3 _ O_2,O_8
86	1527	1446	44.1	1341(m)	β CC_{R1}
87	1560	1477	0.9		β CH_{R2}
88	1649	1562	4.9	1512(s)	β CH_{R2}
89	1668	1580	279.1	1556(vs)	β CC_{R1}
90	1674	1585	313.7	1576(vs)	β CC_{R1}
91	1686	1596	75.8		β CC_{R2}
92	1701	1611	273.3	1611(vs)	ν C=C
93	1792	1697	168.4	1649(s)	ν C=O
94	3033	2872	41.6		ν sym CH_3 of CH_3-O_2
95	3035	2874	32.4	2924(m)	ν sym CH_3 of CH_3-O_8
96	3063	2900	19.0		ν sym CH_3 of CH_3-C
97	3101	2937	1.0		ν asym CH_2 of CH_3 – O_2 and CH_3 – O_2
98	3101	2937	47.4	2956(m)	ν asym CH_2 of CH_3 – O_2 and CH_3 – O_2

Table 4 (continued)

Mode no.	Unscaled freq.	Scaled freq.[a]	$I^{Infrared}$	FT-IR[b]	IR assigments
99	3129	2963	6.8		ν asym CH_2 of CH_3 – C
100	3146	2980	9.1		ν asym CH_3 –C
101	3161	2994	15.3		ν asym CH_3–O_2
102	3163	2996	0.1		ν C_6H_6
103	3174	3005	16.5		ν asym CH_3 – O_8
104	3175	3007	8.8		ν $C_{16}H_{16}$
105	3179	3010	8.9		ωC_5H_5+ω $C_{18}H_{18}$
106	3196	3027	1.7		ν C_5H_5+ν C_7H_7+ν $C_{18}H_{18}$
107	3203	3033	0.1		ν $C_{15}H_{15}$
108	3209	3039	3.1		ν $C_{17}H_{17}$
109	3212	3042	5.9		ν C_5H_5+ν C_7H_7
110	3224	3053	0.5		ν $C_{11}H_{11}$
111	3233	3061	3.7	3215(m)	ν C_9H_9+ν C_7H_7

R1 and R2; first and second ring, ν; stretching, β; in plane bending, ; out of plane bending, ρ; scissoring, Γ; torsion, ω; wagging, r; rocking, t; twisting IR intensities, [$I^{Infrared}$ (K mmol−1)]

[a] Scale factor 0.947

[b] Intensity: vs; very strong, s; strong, m; medium, w; weak, vw; very weak

H_3CO and CH_3 groups. These orbitals are π-bonding and π-antibonding character, respectively. The high gap energy (2.3045 eV) indicate that this compound has high chemical stability and high excitation energies.

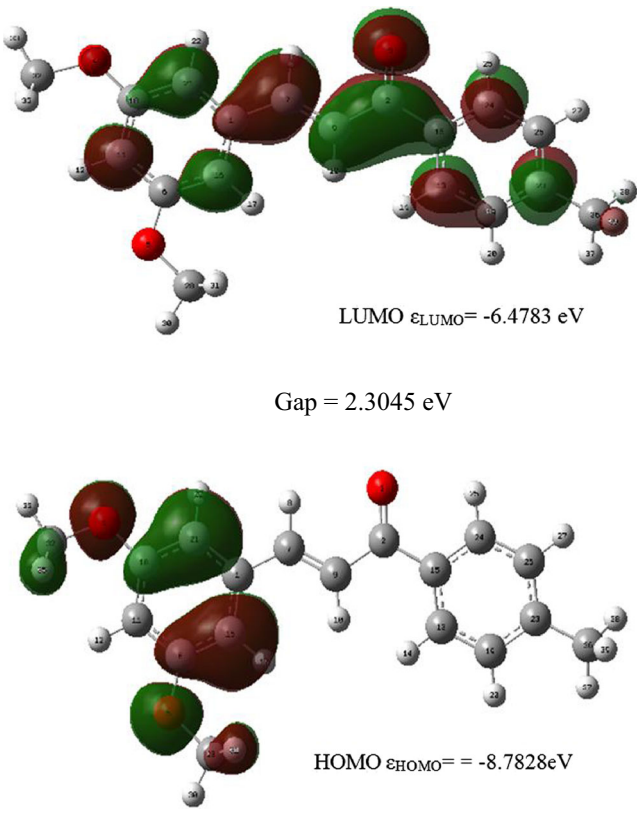

Fig. 5 The HOMO and LUMO distribution of $C_{18}H_{18}O_3$ by using M062X. Gap 2.3035 eV

The hardness (η) of a molecule is given by [32]:

$$\eta = \frac{E_{LUMO} - E_{HOMO}}{2},$$

where E_{LUMO} and E_{HOMO} are the energies of the LUMO and HOMO orbitals, respectively. The chemical hardness is directly correlated to the chemical stability. The molecules having a small or large energy gap are known as soft or hard molecules, respectively. The hard molecules are not more polarizable than the soft ones because they need a big energy to excitation [36]. The value of the energy gap between the HOMO and LUMO is 2.3045 eV and the value of hardness is

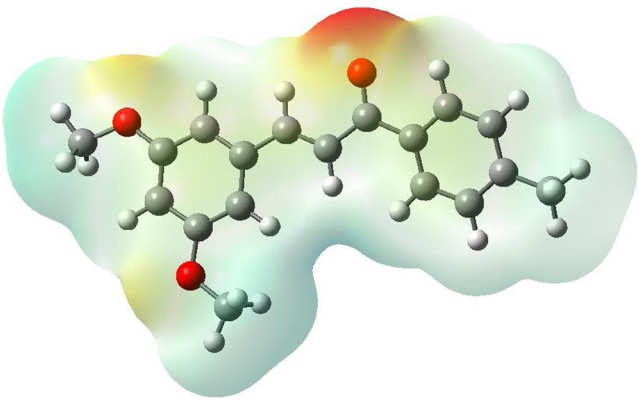

Fig. 6 Potential electrostatic surface calculated at M062X/6-311+G*.Electrostatic potential maps calculated on the Connolly surfaces of the chalcone derivatives from sub negative electrostatic potential regions are represented in red (high electronic density) while positive electrostatic potential areas are shown in dark blue (low electronic density)

1.1522 eV. Compared to the (E)-4-methoxy-2-[(ptolylimino)methyl]phenol molecule [36], which is a Schiff based compound (1.842 eV), the studied molecule presents a smaller hardness.

Electrostatic potential surface

The MEP is associated to the electronic density and it is an important property to explain sites of reactivity as well as their interactions [37]. The negative MEP corresponds to the areas of high electron density; which are in the vicinity of the carbonyl and ethoxyl oxygen atoms (red color in Fig. 6). Thus, the MEP is also a useful property to provide the specific information about the processes of interaction of one molecule with another. Electric charges in the molecule are the driving force for electrostatic interactions [38]. The electrostatic potential surface plotted in Fig. 6 shows regions that are well distinguished. Close to the oxygen atoms there is a negative charge concentration, although close to the hydrogen atoms there is a high concentration of positive charges. This behavior contributes to link the molecules in the packing environment [38].

Conclusions

The compound $C_{18}H_{18}O_3$ was crystallized in the centrosymmetric space group $P2_1/c$, and the DFT analysis of optimized structural parameters showed good agreement to those observed in X-ray diffraction. The molecules are connected by C-H…O hydrogen bonds and the short contacts of the type π…π and C—O…π help the crystal packing stabilization. The Hirshfeld surface analysis with finger plots and electrostatic potential map reveals the percentage of intermolecular contacts and distribution of electrostatic potential. This diagram helps to understand the reactive behavior of the compounds.

The vibrational FT-IR spectrum of molecule was recorded and assigned with the aid of the experimental and computed vibrational wavenumbers. The comparison of the predicted bands with the experimental results shows an acceptable general agreement. The frontier molecular orbital's and potential electrostatic surface calculated are parameters that provide evidence of the lock and key mechanism on any chemical or biological process that could be of interest. Also, they showed how aromatic rings are regions more likely to interact with nearest neighbor molecule. In summary, a structural characterization of title compound was given in the present paper showing that the M06-2X hybrid density functional are able to supply a variety of very reliable molecular properties.

Acknowledgments The authors would like to acknowledge the following Brazilian agencies for financial support: Conselho Nacional de Desenvolvimento Científico e Tecnológico (CNPq) and Fundação de Amparo Pesquisa do Estado de Goiás (FAPEG).

References

1. Rao YK, Fang SH, Tzeng YM (2009) Synthesis and biological evaluation of 3′,4′,5′-trimethoxychalcone analogues as inhibitors of nitric oxide production and tumor cell proliferation. Bioorg Med Chem 17(23):7909–7914
2. Wu J et al. (2012) Synthesis and crystal structure of chalcones as well as on cytotoxicity and antibacterial properties. Med Chem Res 21(4): 444–452
3. Juvale K, Pape VFS, Wiese M (2012) Investigation of chalcones and benzochalcones as inhibitors of breast cancer resistance protein. Bioorg Med Chem 20:346–355
4. Liu M, Wilairat P, Croft SL, Tand ALC, Goa ML (2003) Bioorg Med Chem 11:2729–2738
5. Trivedi JC, Bariwal JB, Upadhyay KD, Naliapara YT, Joshi SK, Pannecouque CC, Clercqd ED, Shah AK (2007) Improved and rapid synthesis of new coumarinyl chalcona derivates and their antiviral activity. Tetrahedron Lett 48:8472–8474
6. Bandgar BP, Gawande SS, Bodade RG, Totre JV, Khobragade CN (2010) Synthesis and biological evaluation of simple methoxylatedchalcones as anticancer, anti-inflammatory and antioxidant agents. Bioorg Med Chem 18:1364–1370
7. Katsori AM, Hadjipavlou-Litina D (2011) Recent progress in therapeutic applications of chalcones. Exp Opin Ther Patents 21:1575–1596. doi:10.1517/13543776.2011.596529
8. Edward HK, Li D (2008) Drug-like properties: concepts, structure design and methods. Elsevier, San Diego
9. Basavoju S, Boström D, Velaga S (2008) Indomethacin–saccharin cocrystal: design, synthesis and preliminary pharmaceutical characterization. Pharm Res 25(3):530–541
10. Silverman RB (1992) The organic chemistry of drug design and drug action. Elsevier, San Diego
11. Enraf-Nonius (1993) CAD-4=PC 1.2 Enraf-Nonius. Delft, Netherlands
12. Sheldrick GM (1990) SHELXS-97 Program for the solution of crystal structures. University of Gottingen, Germany
13. Enraf-Nonius (2000) COLLECT Nonius BV. Delft, Netherlands
14. Otwinowski Z, Minor W (1997) Processing of X-ray diffraction data collected in oscillation mode. In: Carter CWJ (ed) Methods in enzymology, vol 287. Academic, San Diego, pp 307–326
15. Farrugia L (1999) WinGX suite for small-molecule single-crystal crystallography. J Appl Crystallogr 32(4):837–838
16. Farrugia L (1997) ORTEP-3 for Windows - a version of ORTEP-III with a Graphical User Interface (GUI). J Appl Crystallogr 30:565–1997
17. Macrae CF et al (2006) Mercury: visualization and analysis of crystal structures. J Appl Crystallogr 39(3):453–457
18. Spackman MA, McKinnon JJ (2002) Fingerprinting intermolecular interactions in molecular crystals. Cryst Eng Comm 4(66):378–392
19. McKinnon JJ, Spackman MA, Mitchell AS (2004) Novel tools for visualizing and exploring intermolecular interactions in molecular crystals. Acta Crystallogr B 60(6):627–668
20. Wolff SK et al (2007) Crystal Explorer 2.1. University of Western Australia, Perth, Australia
21. Frisch MJ et al. (2004) Gaussian 03 Revision C02. Gaussian Inc, Wallingford, CT
22. Frisch MJ et al (2009) Gaussian Inc. Wallingford, CT

23. Zhao Y, Truhlar DG (2008) The M06 suite of density functionals for main group thermochemistry, thermochemical kinetics, noncovalent interactions, excited states, and transition elements: two new functionals and systematic testing of four M06-class functionals and 12 other functionals. Theor Chem Account 120:215–241
24. GaussView, Version 5, Dennington R, Keith T, Millam J (2009) Semichem Inc, Shawnee Mission
25. Krishnan R, Binkley JS, Seeger R, Pople JA (1980) J Chem Phys 72: 650
26. Frisch MJ, Pople AJ, Binkley JS (1984) J Chem Phys 80:3265
27. Politzer P, Murray JS (2002) Theor Chem Acc 108:134
28. Scott AP, Radom L (1996) J Phys Chem 100:16503–16513
29. Russell D. Johnson III, (2013), NIST computational chemistry comparison and benchmark database. IOP Publishing web. http://cccbdb.nist.gov/vibscale2.asp?method=58&basis=1. Accessed 26 Mar 2014
30. Silverstein M, Basseler GC, Morill C (1981) Spectrometric identification of organic compounds. Wiley, New York
31. Lin-Vien D, Colthup NB, Fateley WG, Grasselli JG (1991) The handbook of infrared and Raman characteristic frequencies of organic molecules. Academic, Boston
32. Pearson RG (1986) Absolute electronegativity and hardness correlated with molecular orbital theory. Proc Natl Acad Sci U S A 83:8440–8441
33. Sklenar H, Jager J (1979) Molecular structure-biological activity relationships on the basis of quantum-chemical calculations. Int J Quantum Chem 26:467–484
34. Zhow Z, Parr RG (1990) Activation hardness: New index for describing the orientation of electrophilic aromatic substitution. J Am Chem Soc 112:5720–5724
35. Fukui K (1982) Science 218:747–754
36. Kosar B, Albayrak C (2011) Spectrochim Acta A 78:160–167
37. Singh UC, Kollman PA (1984) An approach to computing electrostatic charges for molecules. J Comput Chem 5(2):129–145
38. Breneman CM, Wiberg KB (1990) Determining atom-centered monopoles from molecular electrostatic potentials. The need for high sampling density in formamide conformational analysis. J Comput Chem 11(3):361–373